JRMP Journal of Radiopharmaceuticals and Molecular Probes Vol. 6, No.1, 2020
J Radiopharm Mol Prob 2020;6(1): 27-38
ISSN 2384-1583(Print) / ISSN 2508-3848(Online)

Review

https://doi.org/10.22643/JRMP.2020.6.1.27

Review of the chemistry of first-generation Tau PET tracers

Ahmed Karam Farag[1], Changkeun Im[1,2], Choong Mo Kang[1*], and Yong Jin Lee[3]

[1] RI Translational Research Team, Division of Applied RI, Korea Institute of Radiological and Medical Sciences (KIRAMS), Seoul, Republic of Korea.
[2] Radiological and Medico-Oncological Sciences, University of Science and Technology, Seoul, Republic of Korea.
[3] Division of Applied RI, Korea Institute of Radiological and Medical Sciences (KIRAMS), Seoul, Republic of Korea.

ABSTRACT

Alzheimer's disease (AD) is one of the challenging conditions that have no cure, yet early diagnosis can help to control the disease. PET imaging of tau has several advantages, such as being a noninvasive, safe diagnostic technique that correlates directly with the disease progression. Many tau tracers have been reported to date; however, the chemical scaffolds of them fall in a narrow chemical window, and none was approved yet as none is entirely selective and sensitive to tau. These problems are being solved as new tracers emerge constantly. In this report, the first-generation tau tracers such as [^{11}C]PBB3, 2-arylquinoline (THK) series, [^{18}F]T808, and [^{18}F]AV-1451 ([^{18}F]T807) are reviewed from an organic and radiochemistry perspective; thus the most effective chemical approach to synthesize these tracers is discussed. This would help to design novel tracers which can meet the challenges faced by the current tracers.

Key Word: Alzheimer's disease, AD, Tau, PET/CT

Introduction

Alzheimer's disease (AD) is a multifactorial chronic disease characterized by loss of memory and, ultimately, death, particularly in the elderly (1). According to Alzheimer's Association 2020 report, AD is the most common form of dementia in old patients, as it comprises up to 80% of the total dementia cases in the US. Recent statistics indicated that AD is the sixth cause of death in the US, and the number of AD patients is expected to increase significantly in the next 30 years. In the US only, total expenses for health care of dementia patients in 2020 is estimated to be $305 billion, which is a burden to any health system (2). For that, billions of dollars are being spent to treat AD; however, all the current marketed therapeutics are merely symptoms-based treatments (3, 4).

Nevertheless, it is believed that early detection of the disease contributes to better management of the symptoms, which benefits the patient ultimately (5). Typically, the level of several biomarkers, such as beta-amyloid (A-β) and tau protein is detected in the cerebrospinal fluid (CSF) (6); however, several pieces of evidence disproved the accuracy of this technique, particularly with the development of several noninvasive, accurate techniques including PET imaging (7, 8). In fact, PET imaging has been extensively applied for the characterization of the severity of AD cases, the progress of the diseases, and the efficacy of the therapeutic approach used.

AD is characterized by two main hallmarks: deposition of extracellular amyloid plaques formed by aggregation of soluble A-β protein to form insoluble plaques, and deposition of intraneuronal neurofibrillary tangles

Received: June 15, 2020 / Revised: June 24, 2020 / Accepted: June 26, 2020

Corresponding Author : Choong Mo Kang, RI Translational Research Team, Division of Applied RI, Korea Institute of Radiological and Medical Sciences, 75 Nowon-ro, Nowon-gu, Seoul 01812, Korea, Tel: +82-2-970-1628, Fax: +82-2-970-1986, Email: ck190@kirams.re.kr

composed of hyperphosphorylated tau tangles that have been dissociated from the microtubules (9). Typically, the concentration of A-β deposits is up to 20-times higher than tau tangles in AD brain, as A-β deposition happens first as AD develops. However, tau tangles were found to correlate better with the clinical symptoms of AD than the deposition of A-β plaques (10, 11). This explains the continuous failure in the clinical trials employing A-β ligands (12). Interestingly, many A-β PET imaging agents were FDA-approved, while no tau radioligands have been approved so far.

Tau PET tracers have been classified into first- and second-generation based on their potency, pharmacokinetics (PK), and selectivity, with the second-generation being superior in those terms. As a rule of thumb, tau tracers should have specific requirements to be suitable for further evaluation in human subjects, which were extensively reviewed in several review articles (13, 14). Those requirements include: (i) being small molecule with molecular weight < 700; (ii) highly potent (nanomolar affinity) and high selectivity to tau filaments over other targets in the brain; (iii) high brain uptake due to high BBB penetration; (iv) not a substrate for efflux transport proteins; (v) fast clearance from the brain with no BBB-penetrant radioactive metabolites. Several radiotracers developed recently have been chosen based on their ability to abide by these regulations.

Even though there are hundreds of reviews about tau tracers for PET imaging, to the best of our knowledge, there are very few discussing the chemical structures or the synthetic approaches to these tracers. In this report, we intend to review the first-generation tau tracers from an organic pharmaceutical chemistry perspective. In other words, chemical structures, chemical synthesis, and radiolabeling of first-generation tau PET ligand will be the focus of this report.

First-generation tau tracers

The main characters that separates first-generation from second-generation tau tracers are their low tau selectivity and high uptake in the subcortical white matter (15). The affinity to monoamine oxidase (MAO)-A and MAO-B as an off-target was found to be a common character in all the first-generation ligands, which is responsible, at least in part, for distorting the PET image obtained using those. A recent molecular modeling study revealed that there is, indeed, a common binding site for all those tracers on MAO-B, which is similar to that of safinamide, a known MAO-B inhibitor (16). Furthermore, while tau is known to accumulate in posterior cingulate, inferior lateral temporal, and lateral parietal regions according to histopathological studies and postmortem data, many members of the first-generation tau tracers showed discrepancy with their PET images in human subjects (14, 17). The radiotracers discussed in this review are described in Fig. 1, which include [^{11}C]-PBB3, 2-arylquinoline series ([^{18}F]THK-5117, [^{18}F]THK-5317, [^{18}F]THK-5151, [^{18}F]THK-5451, and [^{18}F]THK-5351), [^{18}F]AV-1451 ([^{18}F]T807), and [^{18}F] T808

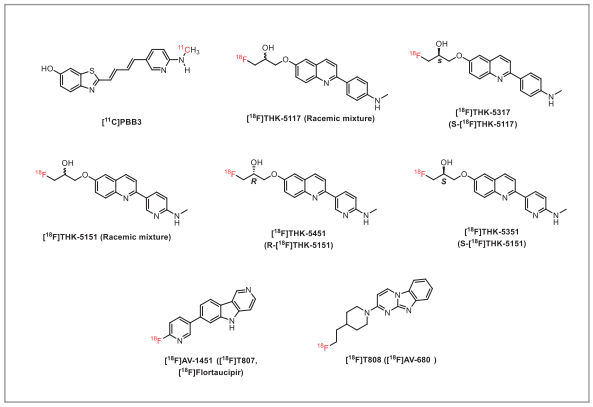

Figure 1. Chemical structure of first-generation tau PET radioligands discussed herein.

[^{11}C]PBB3

The Pyridinyl Butadienyl Benzothiazole [^{11}C]PBB3 tracer is one of the firstly introduced tau ligands that was developed by the National Institute of Radiological Sciences in Japan, based on the structure of the A-β tracer [^{11}C]PiB. Separating the benzothiazole and the aminopyridine moieties in the A-β tracer [^{11}C]AZD2184 with all-trans butadienyl bridge lead to the development of [^{11}C]PBB3 with 2.55 nM affinity to tau protein. Due to similarities in the structure of [^{11}C]PBB3 with other A-β tracers, it is easy to predict that it binds both tau and A-β (only 50-fold selective to tau over A-β). Thus PET imaging with this tracer correlates better to A-β tracers than other tau ligands with higher tau selectivity (18, 19). In addition, the butadienyl linker caused the compound to lose almost 50% of its radiochemical purity within 10 minutes of exposure to fluorescent light by photoisomerization (20). Besides, the preclinical evaluation of [^{11}C]PBB3 revealed significant issues, such as low brain uptake, brain-penetrant metabolites, which limit its applications in humans (21). Furthermore, being a ^{11}C-tracer means that the tracer should only be prepared and used in-house due to the short half-life (20 minutes). Despite those shortcomings, the compound was recently found to be effective in discriminating other forms of tauopathies than AD, such as Progressive Supranuclear Palsy (PSP), corticobasal degeneration (CBD) in addition to α-synucleinopathies (21-23).

Synthesis of cold PBB3 was reported in 2015, starting from 5-bromo-2-nitropyridine (**1**) and 6-methoxy-2-methylbenzothiazole (**4**) as illustrated in **Scheme 1**. (24). Compound **1** was reacted with acrolein diethyl acetal (**2**) adapting Cacchi reaction conditions to yield compound **3** in a moderate 30% yield (25). The commercially available compound **4** was reacted with diethylchlorophosphate using in situ prepared lithium diisopropylamide (LDA) to obtain compound **5** in 67% yield, which was reacted with **3** using Wittig-Horner conditions to afford a 42% yield of compound **6** (26). Metal-catalyzed selective reduction of the nitro group of **6** was achieved, in low yield, using iron, acetic and hydrochloric acids to obtain compound **7**, which was N-monomethylated via condensation with paraformaldehyde followed by sodium borohydride reduction to obtain **8** in moderate 42% yield. Compound **8** was O-demethylated using standard boron tribromide

Scheme 1. Chemical synthesis of PBB3.

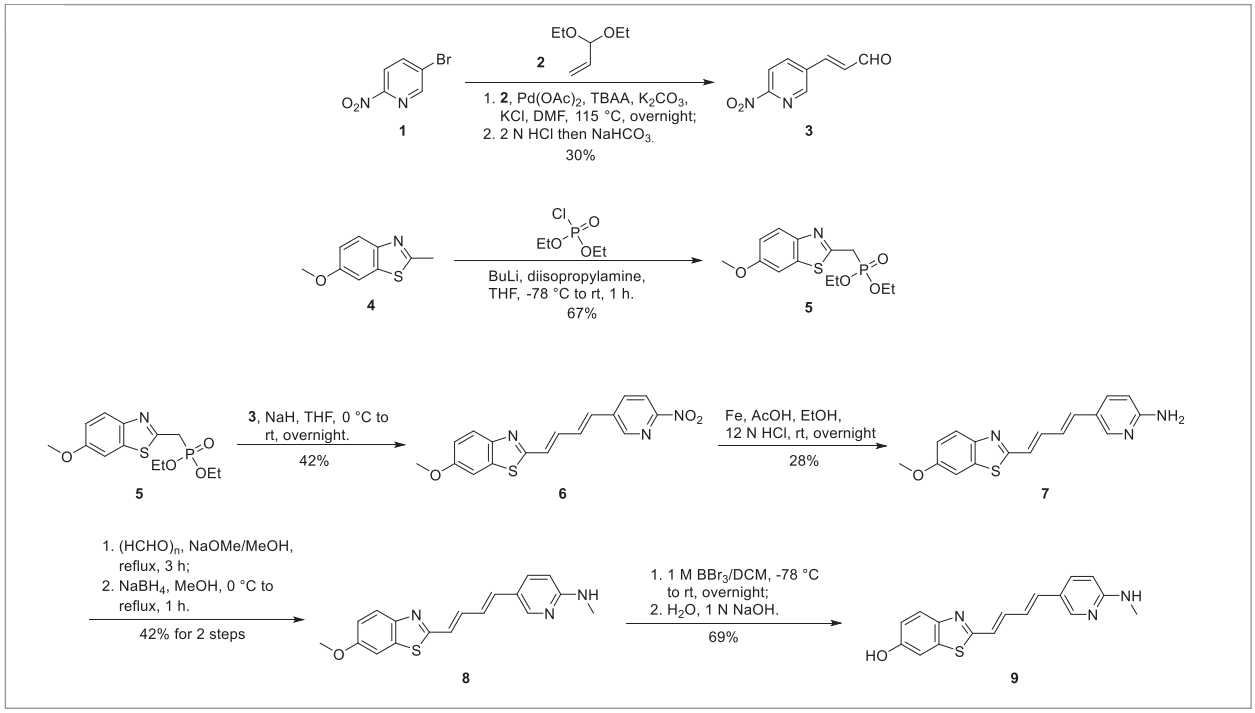

procedure in dichloromethane (DCM) to get the cold PBB3 (**9**) in 69% yield.

Radiolabeling of [^{11}C]PBB3.

Radiosynthesis of [^{11}C]PBB3 is based on mono-methylation of the primary amine on the pyridine ring, as depicted in **scheme 2**. In general, the amino group in the α-position of a pyridine ring is weekly nucleophilic due to the mesomeric and inductive effects of the pyridine nitrogen. Therefore, harsh reaction conditions might be required to methylate this primary amine. However, extremely harsh conditions might result in demethylation, which means that the reaction conditions must be optimized. The decay corrected radiochemical yield (DCRY) of the synthesized [^{11}C]PBB3 was affected by the type of precursor (O-t-butyldimethylsilyl (TBS) protected or unprotected precursor) and reagents ([^{11}C] MeOTf or [^{11}C]MeI) used. In the case of TBS protected precursor, the use of either reagent gave rise to 15–20% DCRY, while the use of unprotected reagent with [^{11}C] MeOTf increased the DCRY to 20–25%. Although there were some variations between the two protocols that used the O-TBS-protected precursor in terms of reaction temperature and reaction time (**scheme 2**), both procedures gave comparable DCRY (20, 24).

Demethylation of the methoxy group in compound **7** using standard boron tribromide procedure afforded compound **10** in 71 % yield. Free phenolic hydroxyl group in compound **10** was protected by TBS group to afford compound **11** in 33% yield, which was used as the precursor for the radiolabeling of [^{11}C]PBB3. Alternatively, unprotected compound **7** was applied directly to prepare [^{11}C]PBB3 (24). To acetone solution of **7** was added KOH, and [^{11}C] MeOTf was passed for 2 minutes at room temperature. The reaction mixture was heated to 80 °C for 5 minutes, quenched with water, and finally purified using high performance liquid chromatography (HPLC) to obtain [^{11}C] PBB3.

The 2-arylquinoline (THK) series

[^{18}F]THK-5117, [^{18}F]THK-5151, [^{18}F]THK-5317, [^{18}F] THK-5351 and [^{18}F]THK-5451

In 2005, Okamura et al. reported the first development of a series of tau tracers based on quinoline scaffold (27). Followed that, many trials to improve the potency, the selectivity to tau, and the PK parameters were attempted, ultimately leading to the discovery of what is considered now among the most extensively studied tau tracers in human. The THK series members used in human studies

Scheme 2. Efficient radiolabeling approach to [^{11}C]PBB3.

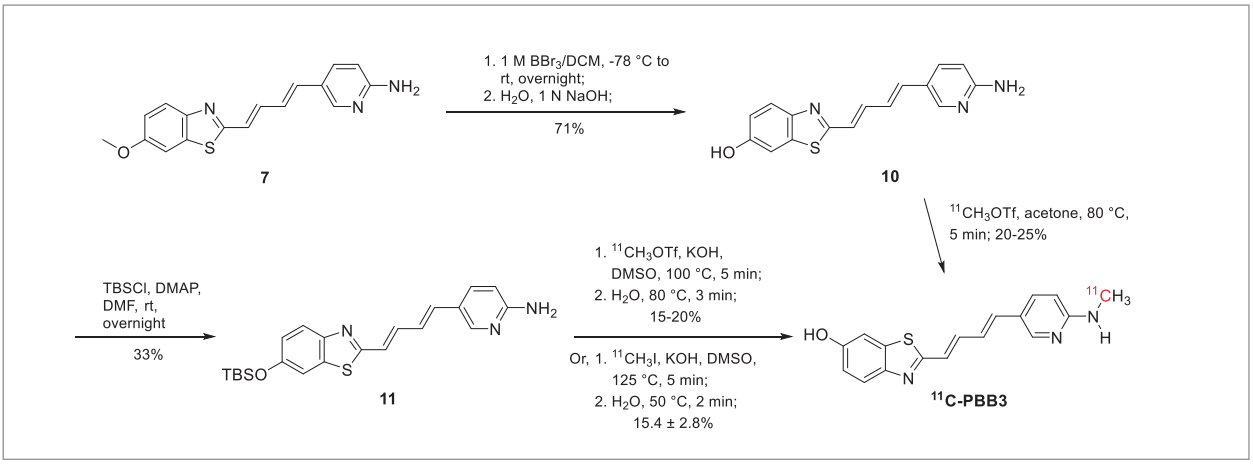

or currently undergoing clinical trials include [^{18}F]THK-5117 and [^{18}F]THK-5151, both contain a chiral center at the secondary alcohol carbon. This chirality gives rise to two enantiomers for each of the compounds with differences in their biological behavior. For [^{18}F]THK-5151, studies have shown that the S-enantiomer ([^{18}F]THK-5317) has superior PK to its R-isomer and consequently was further subjected to intensive studies (28, 29). The strategic introduction of N atom to the phenyl on the 2-position of the quinoline ring resulted in [^{18}F]THK-5351. This minor structural modification resulted in significant improvement of the overall PK of the [^{18}F]THK-5351 over [^{18}F]THK-5117 (30-32).

The chemical synthesis of the racemates THK-5151 and THK-5117 starts with chlorination of the commercial quinoline-2,6-diol using thionyl chloride in dimethylformamide (DMF), which converts the 2-hydroxy into chloro substituent in 86% yield **(Scheme 3)**. The weekly phenolic hydroxy group on position 6 is not affected by these conditions. This led to compound **13**, which was etherified at the 6-hyroxy group with a racemic mixture of 2-((t-butyldimethylsilyl)oxy)-3-fluoropropan-1-ol (compound **14**) to obtain compound **15** in 86% yield. Compound **15**, as a key intermediate, was used to prepare THK-5151 and THK-5117 by applying Suzuki coupling conditions according to the boronate/boronic acid used. Reacting compound **15** with (6-fluoropyridin-3-yl)boronic acid (**16**) yielded compound **17** in an excellent 94% yield, which was further deprotected using straightforward use to fluoride-bearing tetrabutylammonium fluoride to remove the silicon-based TBS group (95% yield). Aromatic nucleophilic substitution of the fluoro atom on the 2-position of the pyridine ring with methylamine in methanol gave rise to THK5151 in 85% yield as a racemic mixture.

Scheme 3. Chemical synthesis of the racemic mixture THK-5151.

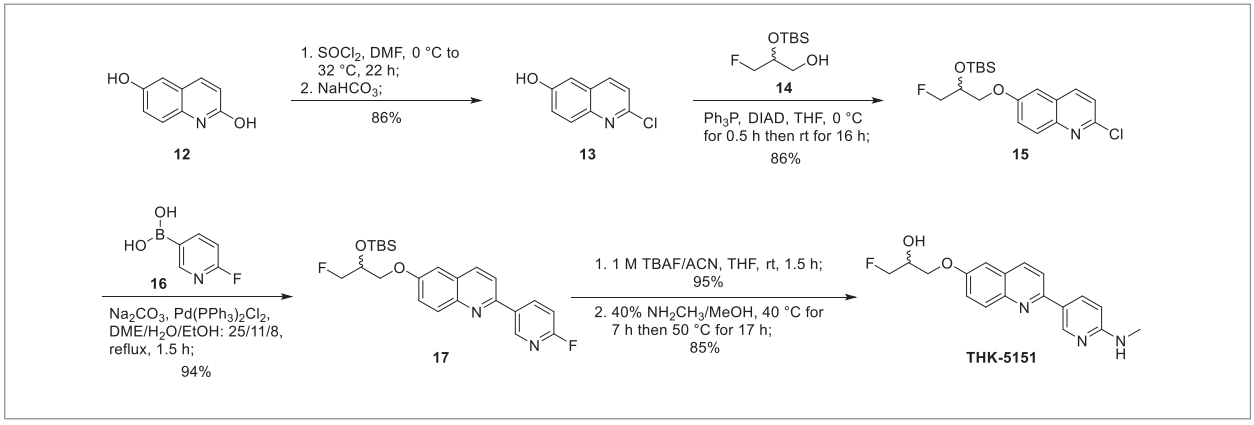

Scheme 4. Synthetic steps for construction of THK-5117 racemic mixture and chiral resolution of [^{18}F]THK-5117 to obtain [^{18}F]THK-5317.

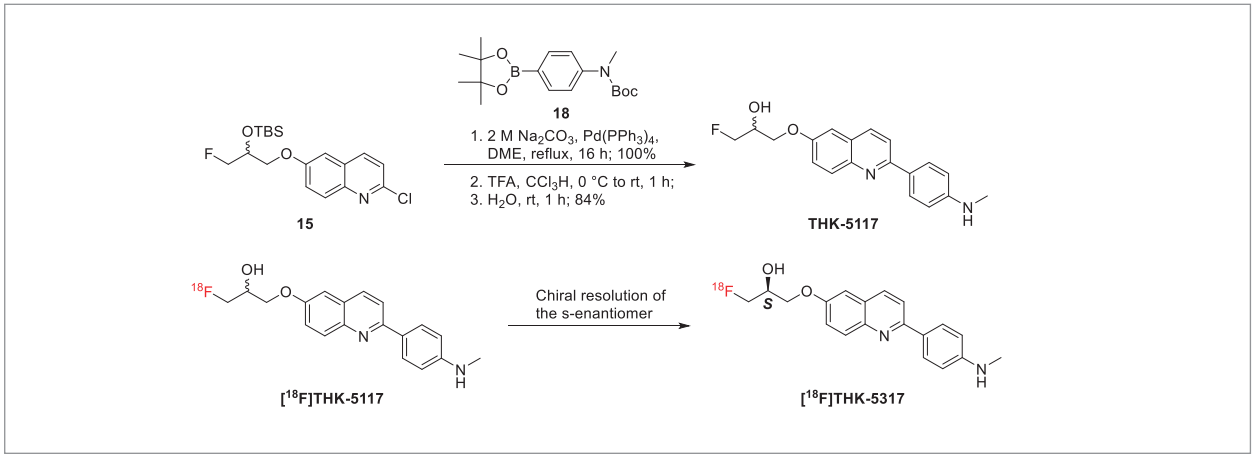

Scheme 5. Radiochemical synthesis of [^{18}F]THK-5117 and [^{18}F]THK-5351.

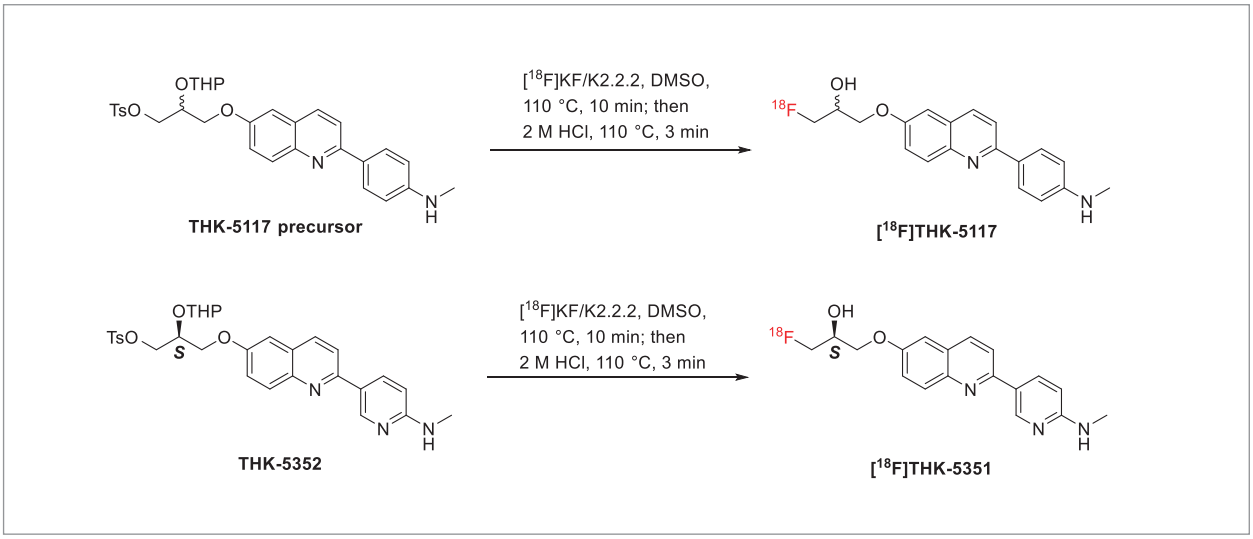

Alternatively, refluxing compound **15** with the pinacolato boronate ester **18** under Suzuki coupling conditions afforded a quantitative yield of the di-protected THK-5117 that was deprotected under acidic conditions of TFA to obtain THK-5117 in 84% yield as a racemic mixture as shown in **Scheme 4**. Chiral separation of the racemic mixture [^{18}F]THK-5117 gave rise to [^{18}F]THK-5317.

Radiolabeling of [18F]THK series

Aliphatic and aromatic radiolabeling reactions with ^{18}F, in the form of [^{18}F]KF, are generally based on nucleophilic substitution mechanism using a suitable leaving group in the site required to be labeled in the precursor. Because of the poor nucleophilicity of the fluoride anion (F^-), a catalyst is generally required. Kryptofix 2.2.2 (K2.2.2). is a cyclic ether-amine-based potassium ion chelator. The use of K2.2.2 with KF significantly improves the nucleophilicity of the F^- allowing the nucleophilic substitution reaction to proceed at reasonable reaction conditions. Therefore, the general procedure to activate the [^{18}F]F^- involves the addition of acetonitrile solution K2.2.2 to the K_2CO_3 solution of the [^{18}F]F^- followed by azeotropic evaporation at 110 °C in order to obtain the anhydrous form of [^{18}F]KF/K2.2.2 complex which is the activated form of [^{18}F]F^- that is suitable for fluorination reaction. THK-5117 precursor is then dissolved in dimethyl sulfoxide (DMSO) and heated with the activated [^{18}F]F^- at 110 °C for 10 minutes to prepare [^{18}F]THK-5117 (**Scheme 5**). Deprotection of the O-protecting THP group is then achieved by adding 2 M HCl to the reaction mixture and allow it to react for 3 more minutes (33).

Betthauser et al. reported the synthesis of [^{18}F]THK-5351 using a similar reaction condition, but they also found that the increase in radiolabeling was minimal after 7 minutes following **scheme 5**. The DCRY obtained by this method was 23–55% depending on the mass of the precursor used; large amount of precursor gave higher yield (34). Neelamegam et al. reported automated radiolabeling of [^{18}F]THK-5351 following a 2-steps one-pot reaction as depicted in **Scheme 5**. with 21.0 ± 3.5% non-decay-corrected radiochemical yield (35). Fully automated radiolabeling of [^{18}F]THK-5351 with high yield was reported by Lee et al. In this report, [^{18}F]F^- was activated with potassium methanesulfonate (pH 7.8)/ K2.2.2 and dried azeotropically with acetonitrile. The solution of the THK-5352 precursor in DMSO was added and the reaction was progressed under the same standard conditions illustrated in **Scheme 5**. The total process time was 75.0 ± 5.0 min, including HPLC purification and formulation to obtain [^{18}F]THK-5351 in a non-decay-corrected radiochemical yield of 31.9 ± 11.1% (36).

Siemens series ([^{18}F]T807 and [^{18}F] T808)

[^{18}F]AV-1451 ([^{18}F]T807, [^{18}F]Flortaucipir)

Between 2011 and 2013, the molecular imaging biomarker research team in Siemens Medical Solutions reported two radiotracers, [^{18}F]T807 and [^{18}F]T808. [^{18}F] T807 was developed by Avid Radiopharmaceuticals and currently belongs to Eli Lilly pharmaceuticals. Today, these two tracers are the most extensively studied tau tracers due to their high nanomolar affinity to tau paired helical filaments (PHFs), reasonable selectivity to tau PHF, good PK properties and low binding to the white matter (37, 38). The chemical nucleus is different between both tracers. Whereas [^{18}F]T807 has a pyrido[4,3-b]indole scaffold, [^{18}F]T808 core is a benzo[4,5]imidazo[1,2-a] pyrimidine. Furthermore, [^{18}F]T807 bears an aromatic [^{18}F]fluoro atom, while [^{18}F]T808 has an aliphatic one. This means that the chemical synthesis and radiolabeling pathways are different. Besides, the two tracers shall have different kinetics and metabolism. It is also noteworthy to mention that [^{18}F]T807 does not contain an aliphatic fluoro atom, but rather an aromatic fluoro, which is more stable to oxidative defluorination metabolism compared to [^{18}F] T808. This led to the selection of [^{18}F]T807 for further clinical evaluation over [^{18}F]T808 (39).

The synthesis of the pyrido[4,3-b]indole scaffold-containing T807 was achieved via refluxing the commercially available 3-bromo-4-nitropyridine (**19**) with 4-bromophenylboronic acid (**20**) using Suzuki coupling standard procedure to obtain compound **21** in good yield (72%) as illustrated in **Scheme 6** (40). Reductive cyclization of **21** using triethyl phosphite resulted in a comparatively higher yield (70%) of the key intermediate **22**. This higher-than-expected yield was achieved by controlling the time and the temperature of the cyclization reaction. Next, **22** was subjected to a second round of Suzuki coupling reaction with compound **16**, which afforded T807 in 53% yield. Alternatively, the Stille cross-coupling reaction was employed via refluxing 2-nitro-5-(trimethylstannyl)pyridine (**23**) with compound **22** to obtain the unprotected **24**, which was t-butyloxycarbonyl (Boc)-protected to achieve a high yield of compound **24** (85%), which was used as a precursor

Scheme 6. Chemical synthesis and radiolabeling of T807 and [^{18}F]T807.

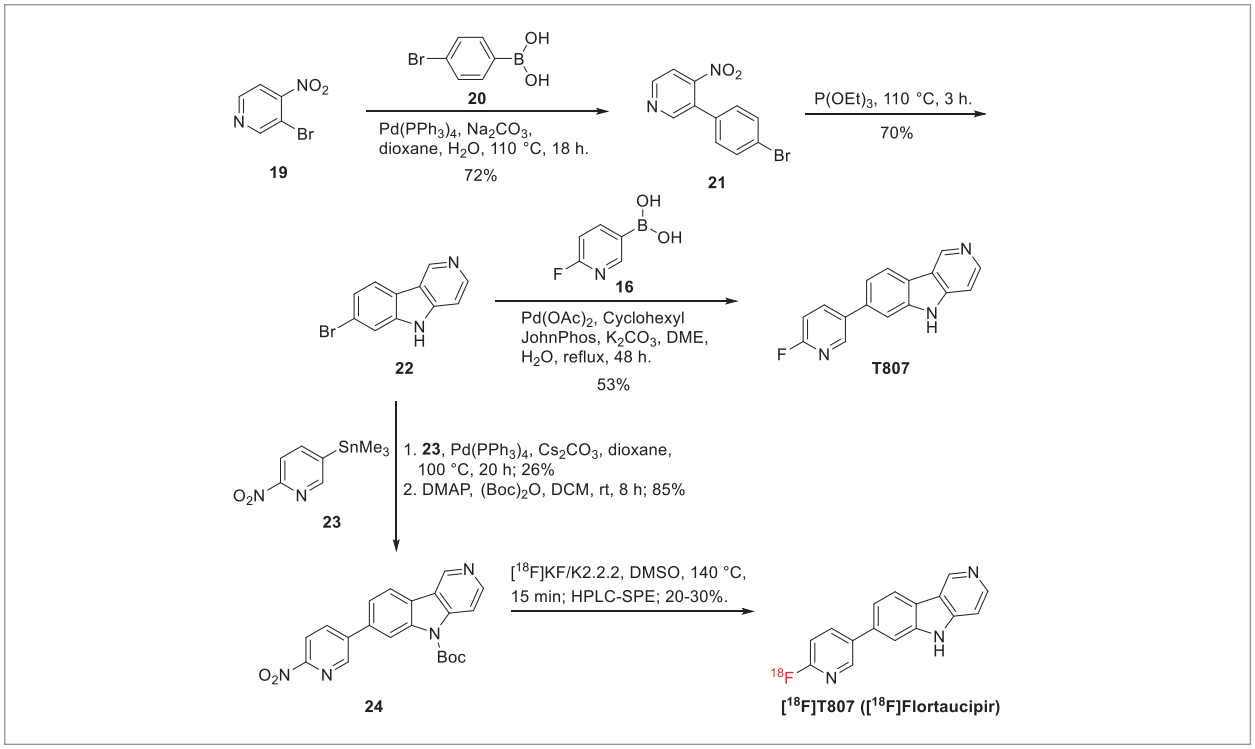

to prepare [^{18}F]T807 (**Scheme 6**).

Radiolabeling of [^{18}F]T807

The radiolabeling of [^{18}F]T807 is a straightforward, fully automated process using compound **24** as the precursor. The process starts with the typical activation of the [^{18}F]F$^-$ using K2.2.2. The activated [^{18}F]F$^-$ (anhydrous [^{18}F]KF/K2.2.2 complex) replaces the nitro group on position 2 of the pyridine of compound **24**. This is achieved by heating a DMSO solution of the precursor **24** with [^{18}F]KF/K2.2.2 complex at 140 °C for 15 minutes, which deprotected the Boc group simultaneously (**Scheme 6**). Shoup et al. and Mossine et al. reported a one-step automated synthesis of [^{18}F]T807 using [^{18}F]KF/K2.2.2 complex in DMSO at 130 °C for 10 minutes. The non-decay-corrected radiochemical yield was comparable in both reports, yet relatively low (14 ± 3%) (41, 42). Gao et al. reported the use of the same precursor **24** in a fully automated radiolabeling and [^{18}F]T807 was obtained after standard quenching at 90 °C with $NaHCO_3$, HPLC purification, and formulation into a sterile product with an improved DCRY of 20–30% (**Scheme 6**) (40).

Holt et al. reported a microwave-assisted synthesis of [^{18}F]T807 using a different precursor, as illustrated in **Scheme 7**. In a microwave vial containing anhydrous [^{18}F]KF/K2.2.2 complex, acetonitrile solution of T807P was added, followed by microwave irradiation for 30 seconds at 50 watts. Deprotection of the Boc group occurred after the addition of 1 N HCl to the microwave vial and

Scheme 7. Radiolabeling of [^{18}F]T807 using assisted microwave-assisted 2-step synthesis.

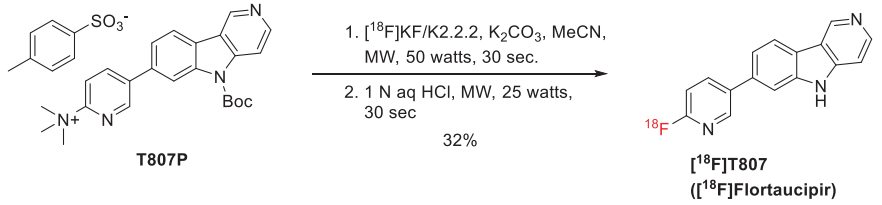

Scheme 8. Chemical and radiolabeling approaches to T808 and [^{18}F]T808 ([^{18}F]AV-680).

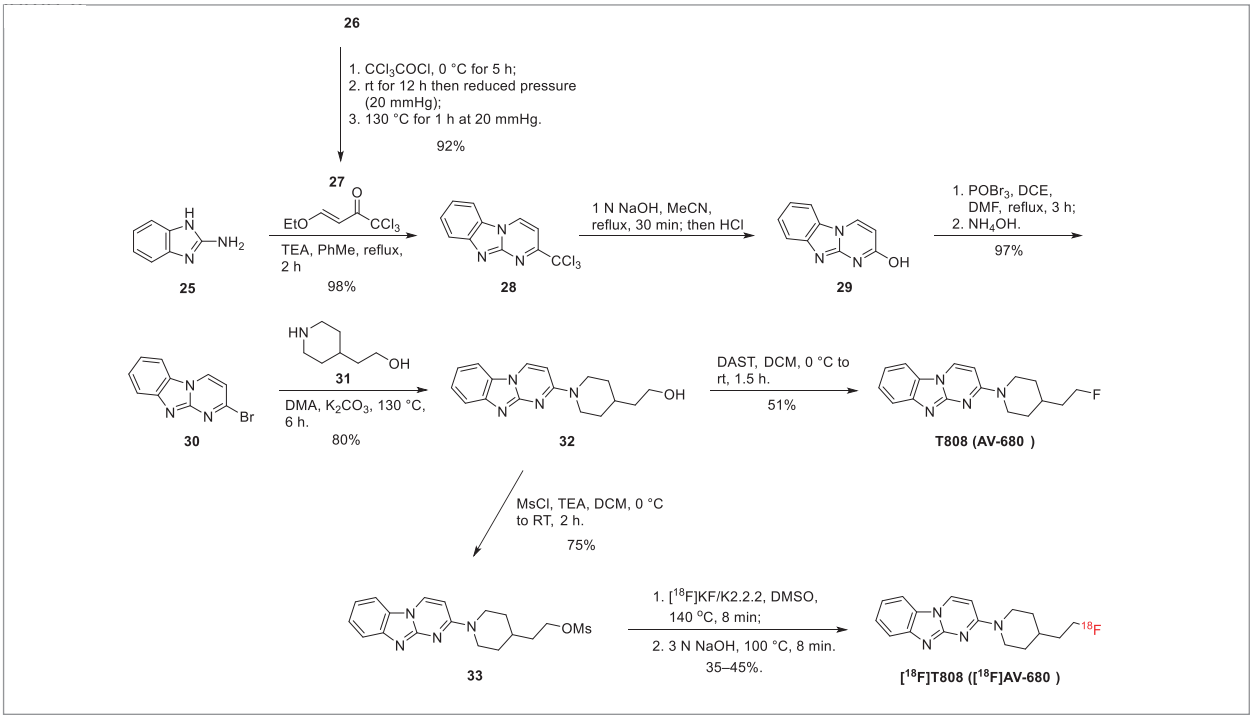

irradiating for 30 seconds at 25 watts. Work up, HPLC purification and formulation gave rise to an average non-decay-corrected yield of 31.9 ± 12.3% after the average 48-minutes synthesis time (43).

[^{18}F]AV-680 ([^{18}F]T808)

AV-680 is based on a benzo[4,5]imidazo[1,2-a]pyrimidine scaffold, which was constructed starting with the commercial 2-aminobenzimidazole (**25**) by some modifications of the original synthetic procedure in order to improve the product yield (**Scheme 8**) (44-46). The highly reactive Michael's acceptor (E)-1,1,1-trichloro-4-ethoxy-but-3-en-2-one (**27**) was synthesized in excellent yield from vinyl ethyl ether and trichloroacetyl chloride by stirring overnight. The resulting **27** was reacted with **25** via a base-catalyzed nucleophilic addition-cyclization mechanism to construct the core benzo-imidazo-pyrimidine scaffold in compound **28** in an almost quantitative yield. Alkaline hydrolysis followed by oxidative decarboxylation of **28** led to the conversion of the trichloromethyl group into hydroxyl group in compound **29** in a nearly quantitative yield. Next, the internal nucleophilic substitution (S_Ni) mechanism was used to substitute the hydroxyl group of **29** to bromo atom in the key intermediate 30 in 97% yield after alkaline neutralization. The 2-bromo substituent of compound **30** was substituted with an N nucleophile in the piperidine reagent **31**. To proceed with this crucial step, several conditions were used, including the microwave use, different solvents, such as dimethyl acetamide (DMA), DMF, and DMSO, a variety of bases, such as potassium carbonate, sodium hydroxide, or even neat uncatalyzed reaction. The highest practical yield was obtained using K_2CO_3 as a base catalyst in DMA, which was 80% of compound **32** in a gram-scale reaction. Following that, the hydroxyl group in compound **32** was substituted using diethylaminosulfur trifluoride (DAST) in DCM to obtain the cold T808 in 51% yield. Alternatively, this hydroxy group was protected using methanesulfonyl chloride to get the mesyl protected compound **33**, which is the precursor for the synthesis of [^{18}F]T808 (**Scheme 8**).

Radiolabeling of [^{18}F]T808

The radiofluorination reaction of compound **33** to obtain [^{18}F]T808 was reported in 2014 by Siemens Molecular Imaging team. Following the standard procedure of activating the F^- in the form of anhydrous [^{18}F]KF/K2.2.2 complex, compound **33** in DMSO was added, and the mixture was heated to 90 °C for 5 minutes. Hydrolysis of the unreacted precursor **33** by refluxing the crude mixture with 3 N NaOH at 100 °C for 10 minutes ensured an effective separation between the precursor **33** and [^{18}F] T808 during HPLC purification. The average DCRY of this synthetic procedure was 37% (39). Gao et al. modified the conditions of the reaction by heating in DMSO at 140 °C for 8 minutes and after that refluxing with 3 N NaOH at 100 °C for 8 minutes. This led to a higher DCRY which was 35–45% (44).

Final remarks and future prospects

Tau PET imaging is an indispensable diagnostic tool for AD patients because it was proven effective in diagnosing the clinical stage of AD-dementia. However, to date, there is no selective tau tracer that is devoid of off-target binding discovered yet, which urges fast-pace research to develop PET tau tracers suitable for commercial human use. In 2017, Fitzpatrick et al. used cryogenic electron microscopy (cryo-EM) to reveal the core structure of tau straight filaments (SF) and PHF at 3.4–3.5 Å resolution (PDB id: 5O3T and 5O3L, respectively) from a sample obtained from an AD patient's postmortem brain tissues

(47). We believe that this discovery will advance the research on this hot topic. In this mini-review, we have mined the literature to present the recent and most effective chemical and radiochemical methods to prepare the first-generation tau PET tracers. Even though there are plenty of molecules developed both in academia and industry, we have focused on the extensively studied tracers as those can set the basis for further development into better tracers.

Acknowledgements

This study was supported by a grant of the Korea Institute of Radiological and Medical Sciences (KIRAMS), funded by Ministry of Science and ICT (MSIT), Korea (No. 50536-2020). The authors declare no conflict of interest.

References

1. Sengoku R. Aging and Alzheimer's disease pathology. *Neuropathology* 2020;40(1):22-29.
2. 2020 Alzheimer's disease facts and figures. *Alzheimers Dement* 2020;16:391-460.
3. Singh H, Chawla V, Bala R, Dureja H. Current and future of Alzheimer's therapy with the best approach. *CNS Neurol Disord Drug Targets* 2020;19:1.
4. Stower H. Searching for Alzheimer's disease therapies. *Nat Med* 2018;24(7):894-897.
5. Guest FL, Rahmoune H, Guest PC. Early diagnosis and targeted treatment strategy for improved therapeutic outcomes in Alzheimer's disease. In: Guest P, editors. Reviews on new drug targets in age-related disorders. Advances in experimental medicine and biology, vol 1260 : *Springer, Cham*; 2020. p. 175-191.
6. Blennow K. CSF biomarkers for Alzheimer's disease: Use in early diagnosis and evaluation of drug treatment. *Expert Rev Mol Diagn* 2005;5(5):661-672.
7. Ritchie C, Smailagic N, Noel-Storr AH, Ukoumunne O, Ladds EC, Martin S. CSF tau and the CSF tau/ABeta ratio for the diagnosis of Alzheimer's disease dementia and other dementias in people with mild cognitive impairment (MCI). *Cochrane Database Syst Rev* 2017;3:CD010803.
8. Uzuegbunam BC, Librizzi D, Hooshyar Yousefi B. PET Radiopharmaceuticals for Alzheimer's disease and Parkinson's disease diagnosis, the current and future landscape. *Molecules* 2020;25(4):977.
9. Wilcock GK, Esiri MM. Plaques, tangles and dementia. A quantitative study. *J Neurol Sci 1*982;56(2-3):343-356.
10. Mullane K, Williams M. Alzheimer's disease beyond amyloid: Can the repetitive failures of amyloid-targeted therapeutics inform future approaches to dementia drug discovery? *Biochem Pharmacol* 2020;177:113945.
11. Jack CR, Jr., Knopman DS, Jagust WJ, Shaw LM, Aisen PS, Weiner MW, Petersen RC, Trojanowski JQ. Hypothetical model of dynamic biomarkers of the Alzheimer's pathological cascade. *Lancet Neurol* 2010;9(1):119-128.
12. Congdon EE, Sigurdsson EM. Tau-targeting therapies for Alzheimer disease. *Nature Reviews Neurology* 2018;14(7):399-415.
13. Leuzy A, Chiotis K, Lemoine L, Gillberg PG, Almkvist O, Rodriguez-Vieitez E, Nordberg A. Tau PET imaging in neurodegenerative tauopathies-still a challenge. *Mol Psychiatry* 2019;24(8):1112-1134.
14. Ariza M, Kolb HC, Moechars D, Rombouts F, Andrés JI. Tau positron emission tomography (PET) imaging: past, present, and future. *J Med Chem* 2015;58(11):4365-4382.
15. Wang YT, Edison P. Tau Imaging in Neurodegenerative Diseases Using Positron Emission Tomography. *Curr Neurol Neurosci Rep* 2019;19(7):45.
16. Murugan NA, Chiotis K, Rodriguez-Vieitez E, Lemoine L, Agren H, Nordberg A. Cross-interaction of tau PET tracers with monoamine oxidase B: evidence from in

silico modelling and in vivo imaging. *Eur J Nucl Med Mol Imaging* 2019;46(6):1369-1382.

17. Braak H, Thal DR, Ghebremedhin E, Del Tredici K. Stages of the pathologic process in Alzheimer disease: Age categories from 1 to 100 years. *J Neuropathol Exp Neurol* 2011;70(11):960-969.
18. Chiotis K, Stenkrona P, Almkvist O, Stepanov V, Ferreira D, Arakawa R, Takano A, Westman E, Varrone A, Okamura N, Shimada H, Higuchi M, Halldin C, Nordberg A. Dual tracer tau PET imaging reveals different molecular targets for ^{11}C-THK5351 and 11C-PBB3 in the Alzheimer brain. *Eur J Nucl Med Mol Imaging* 2018;45(9):1605-1617.
19. Wood H. Alzheimer disease: [^{11}C]PBB3-a new PET ligand that identifies tau pathology in the brains of patients with AD. *Nat Rev Neurol* 2013;9(11):599.
20. Hashimoto H, Kawamura K, Igarashi N, Takei M, Fujishiro T, Aihara Y, Shiomi S, Muto M, Ito T, Furutsuka K, Yamasaki T, Yui J, Xie L, Ono M, Hatori A, Nemoto K, Suhara T, Higuchi M, Zhang MR. Radiosynthesis, photoisomerization, biodistribution, and metabolite analysis of ^{11}C-PBB3 as a clinically useful PET probe for imaging of tau pathology. *J Nucl Med* 2014;55(9):1532-1538.
21. Maruyama M, Shimada H, Suhara T, Shinotoh H, Ji B, Maeda J, Zhang MR, Trojanowski JQ, Lee VMY, Ono M, Masamoto K, Takano H, Sahara N, Iwata N, Okamura N, Furumoto S, Kudo Y, Chang Q, Saido TC, Takashima A, Lewis J, Jang MK, Aoki I, Ito H, Higuchi M. Imaging of tau pathology in a tauopathy mouse model and in Alzheimer patients compared to normal controls. *Neuron* 2013;79(6):1094-1108.
22. Koga S, Ono M, Sahara N, Higuchi M, Dickson DW. Fluorescence and autoradiographic evaluation of tau PET ligand PBB3 to alpha-synuclein pathology. *Mov Disord* 2017;32(6):884-892.
23. Endo H, Shimada H, Sahara N, Ono M, Koga S, Kitamura S, Niwa F, Hirano S, Kimura Y, Ichise M, Shinotoh H, Zhang MR, Kuwabara S, Dickson DW, Toda T, Suhara T, Higuchi M. In vivo binding of a tau imaging probe, [^{11}C] PBB3, in patients with progressive supranuclear palsy. *Mov Disord* 2019;34(5):744-754.
24. Wang M, Gao M, Xu Z, Zheng QH. Synthesis of a PET tau tracer [^{11}C]PBB3 for imaging of Alzheimer's disease. *Bioorg Med Chem Lett* 2015;25(20):4587-4592.
25. Battistuzzi G, Cacchi S, Fabrizi G. An efficient palladium-catalyzed synthesis of cinnamaldehydes from acrolein diethyl acetal and aryl iodides and bromides. *Org Lett* 2003;5(5):777-780.
26. Zhuang ZP, Kung MP, Kung HF. Synthesis of biphenyltrienes as probes for beta-amyloid plaques. *J Med Chem* 2006;49(9):2841-2844.
27. Okamura N, Suemoto T, Furumoto S, Suzuki M, Shimadzu H, Akatsu H, Yamamoto T, Fujiwara H, Nemoto M, Maruyama M, Arai H, Yanai K, Sawada T, Kudo Y. Quinoline and benzimidazole derivatives: candidate probes for in vivo imaging of tau pathology in Alzheimer's disease. *J Neurosci* 2005;25(47):10857-10862.
28. Jonasson M, Wall A, Chiotis K, Saint-Aubert L, Wilking H, Sprycha M, Borg B, Thibblin A, Eriksson J, Sörensen J, Antoni G, Nordberg A, Lubberink M. Tracer kinetic analysis of (S)-18F-THK5117 as a PET tracer for assessing tau pathology. *J Nucl Med* 2016;57(4):574-581.
29. Chiotis K, Saint-Aubert L, Savitcheva I, Jelic V, Andersen P, Jonasson M, Eriksson J, Luberink M, Almkvist O, Wall A, Antoni G, Nordberg A. Imaging in-vivo tau pathology in Alzheimer's disease with THK5317 PET in a multimodal paradigm. *Eur J Nucl Med Mol Imaging* 2016;43(9):1686-1699.
30. Harada R, Okamura N, Furumoto S, Furukawa K, Ishiki A, Tomita N, Tago T, Hiraoka K, Watanuki S, Shidahara M, Miyake M, Ishikawa Y, Matsuda R, Inami A, Yoshikawa T, Funaki Y, Iwata R, Tashiro M, Yanai K, Arai H, Kudo Y. 18F-THK5351: A novel PET radiotracer for imaging neurofibrillary pathology in Alzheimer Disease. J *Nucl Med* 2016;57(2):208-214.
31. Lemoine L, Gillberg PG, Svedberg M, Stepanov V, Jia Z, Huang J, Nag S, Tian H, Ghetti B, Okamura N, Higuchi M, Halldin C, Nordberg A. Comparative binding properties

of the tau PET tracers THK5117, THK5351, PBB3, and T807 in postmortem Alzheimer brains. *Alzheimers Res Ther* 2017;9(1):96.

32. Betthauser TJ, Lao PJ, Murali D, Barnhart TE, Furumoto S, Okamura N, Stone CK, Johnson SC, Christian BT. In vivo comparison of tau radioligands ^{18}F-THK-5351 and 18F-THK-5317. *J Nucl Med* 2017;58(6):996-1002.
33. Okamura N, Furumoto S, Harada R, Tago T, Yoshikawa T, Fodero-Tavoletti M, Mulligan RS, Villemagne VL, Akatsu H, Yamamoto T, Arai H, Iwata R, Yanai K, Kudo Y. Novel 18F-labeled arylquinoline derivatives for noninvasive imaging of tau pathology in Alzheimer disease. *J Nucl Med* 2013;54(8):1420-1427.
34. Betthauser TJ, Ellison PA, Murali D, Lao PJ, Barnhart TE, Furumoto S, Okamura N, Johnson SC, Engle JW, Nickles RJ, Christian BT. Characterization of the radiosynthesis and purification of [^{18}F]THK-5351, a PET ligand for neurofibrillary tau. *Appl Radiat Isot* 2017;130:230-237.
35. Neelamegam R, Yokell DL, Rice PA, Furumoto S, Kudo Y, Okamura N, Fakhri GE. A report of the automated radiosynthesis of the tau positron emission tomography radiopharmaceutical, [^{18}F]-THK-5351. *J Labelled Comp Radiopharm* 2017;60(2):140-146.
36. Lee SJ, Oh SJ, Cho EH, Kim DH, Furumoto S, Okamura N, Kim JS. Full automatic synthesis of [^{18}F]THK-5351 for tau protein PET imaging in Alzheimer's disease patients: 1 year experience. *J Radioanal Nucl Chem* 2017;314(3):1587-1593.
37. Zhang W, Arteaga J, Cashion DK, Chen G, Gangadharmath U, Gomez LF, Kasi D, Lam C, Liang Q, Liu C, Mocharla VP, Mu F, Sinha A, Szardenings AK, Wang E, Walsh JC, Xia C, Yu C, Zhao T, Kolb HC. A highly selective and specific PET tracer for imaging of tau pathologies. *J Alzheimers Dis* 2012;31(3):601-612.
38. Xia CF, Arteaga J, Chen G, Gangadharmath U, Gomez LF, Kasi D, Lam C, Liang Q, Liu C, Mocharla VP, Mu F, Sinha A, Su H, Szardenings AK, Walsh JC, Wang E, Yu C, Zhang W, Zhao T, Kolb HC. [^{18}F]T807, a novel tau positron emission tomography imaging agent for Alzheimer's disease. *Alzheimers Dement* 2013;9(6):666-676.
39. Chien DT, Szardenings AK, Bahri S, Walsh JC, Mu F, Xia C, Shankle WR, Lerner AJ, Su MY, Elizarov A, Kolb HC. Early clinical PET imaging results with the novel PHF-tau radioligand [F18]-T808. *J Alzheimers Dis* 2014;38(1):171-184.
40. Gao M, Wang M, Zheng QH. Fully automated synthesis of [^{18}F]T807, a PET tau tracer for Alzheimer's disease. Bioorg Med Chem Lett 2015;25(15):2953-2957.
41. Shoup TM, Yokell DL, Rice PA, Jackson RN, Livni E, Johnson KA, Brady TJ, Vasdev N. A concise radiosynthesis of the tau radiopharmaceutical, [^{18}F]T807. *J Labelled Comp Radiopharm* 2013;56(14):736-740.
42. Mossine AV, Brooks AF, Henderson BD, Hockley BG, Frey KA, Scott PJH. An updated radiosynthesis of [^{18}F] AV1451 for tau PET imaging. *EJNMMI Radiopharm Chem* 2017;2(1):7.
43. Holt DP, Ravert HT, Dannals RF. Synthesis and quality control of [^{18}F]T807 for tau PET imaging. *J Labelled Comp Radiopharm* 2016;59(10):411-415.
44. Gao M, Wang M, Zheng QH. Concise and high-yield synthesis of T808 and T808P for radiosynthesis of [^{18}F]-T808, a PET tau tracer for Alzheimer's disease. *Bioorg Med Chem Lett* 2014;24(1):254-257.
45. Szardenings AK, Zhang W, Kolb HC, Cashion DK, Chen G, Kasi D, Liu C, Sinha A, Wang E, Yu C, Gangadharmath UB, Walsh JC. *Patent* US20110182812A1. 2011.
46. Cashion DK, Chen G, Kasi D, Kolb HC, Liu C, Sinha A, Szardenings AK, Wang E, Yu C, Zhang W, Gangadharmath UB, Walsh JC. *Patent* WO2011119565A1. 2011.
47. Fitzpatrick AWP, Falcon B, He S, Murzin AG, Murshudov G, Garringer HJ, Crowther RA, Ghetti B, Goedert M, Scheres SHW. Cryo-EM structures of tau filaments from Alzheimer's disease. *Nature* 2017;547(7662):185-190.